Journal of Neuroscience Research 78:668–682 (2004)

Analysis of K^+ Accumulation Reveals Privileged Extracellular Region in the Vicinity of Glial Cells In Situ

Alexandr Chvátal,[1–3]* Miroslava Anděrová,[1–3] and Eva Syková[1–3]
[1]Department of Neuroscience, Institute of Experimental Medicine, Academy of Sciences of the Czech Republic, Prague, Czech Republic
[2]Department of Neuroscience, Charles University, Second Medical Faculty, Prague, Czech Republic
[3]Center for Cell Therapy and Tissue Repair, Charles University, Prague, Czech Republic

Astrocytes and oligodendrocytes in rat and mouse spinal cord slices, characterized by passive membrane currents during de- and hyperpolarizing stimulation pulses, express a high resting K^+ conductance. In contrast to the case for astrocytes, a depolarizing prepulse in oligodendrocytes produces a significant shift of reversal potential (V_{rev}) to positive values, arising from the larger accumulation of K^+ in the vicinity of the oligodendrocyte membrane. As a result, oligodendrocytes express large tail currents (I_{tail}) after a depolarizing prepulse due to the shift of K^+ into the cell. In the present study, we used a mathematical model to calculate the volume of the extracellular space (ECS) in the vicinity of astrocytes and oligodendrocytes (ESV_v), defined as the volume available for K^+ accumulation during membrane depolarization. A mathematical analysis of membrane currents revealed no differences between glial cells from mouse (n = 59) or rat (n = 60) spinal cord slices. We found that the V_{rev} of a cell after a depolarizing pulse increases with increasing I_{tail}, expressed as the ratio of the integral inward current (Q_{in}) after the depolarizing pulse to the total integral outward current (Q_{out}) during the pulse. In astrocytes with small I_{tail} and V_{rev} ranging from –50 to –70 mV, the Q_{in} was only 3–19% of Q_{out}, whereas, in oligodendrocytes with large I_{tail} and V_{rev} between –20 and 0 mV, Q_{in}/Q_{out} was 30–75%. On the other hand, ESV_v decreased with increasing values of V_{rev}. In astrocytes, ESV_v ranged from 2 to 50 μm^3, and, in oligodendrocytes, it ranged from 0.1 to 2.0 μm^3. Cell swelling evoked by the application of hypotonic solution shifted V_{rev} to more positive values by 17.2 ± 1.8 mV and was accompanied by a decrease in ESV_v of 3.6 ± 1.3 μm^3. Our mathematical analysis reveals a 10–100 times smaller region of the extracellular space available for K^+ accumulation during cell depolarization in the vicinity of oligodendrocytes than in the vicinity of astrocytes. The presence of such privileged regions around cells in the CNS may affect the accumulation and diffusion of other neuroactive substances and alter communication between cells in the CNS.

Key words: astrocytes; oligodendrocytes; potassium tail currents; diffusion; extracellular space

The extracellular space (ECS) in the central nervous system (CNS) is the microenvironment of neurons and glial cells. Dramatic changes in the composition of the ECS occur during neuronal activity, when ions, neurotransmitters, peptides, neurohormones, and metabolites are released into the ECS and diffuse to their targets located on neurons as well as on glial cells. Because the neuroactive substances move by diffusion through the volume of the ECS, this type of signal transmission was called *extrasynaptic* or *volume transmission* (for reviews see Agnati et al., 1995; Syková, 1997; Nicholson and Syková, 1998; Zoli et al., 1999). Extrasynaptic transmission is affected by ECS volume and by diffusion barriers that are formed by fine glial and neuronal processes and molecules of the extracellular matrix (Syková et al., 2000; Syková, 2001). It was shown in a number of studies that the diffusion properties of the ECS dramatically change during development; aging; pathological states such as ischemia, injury, X-irradiation, gliosis, and demyelination; and often in grafted tissue (for review see Syková et al., 2000). There is increasing evidence that diffusion barriers in the extracellular space may affect the membrane properties of glial cells (for review see Chvátal and Syková, 2000).

The first electrophysiological measurements of glial cells revealed that their membranes are highly permeable for K^+ (Kuffler et al., 1966; Orkand et al., 1966) and that the relationship between changes in extracellular K^+ concentration ($[K^+]_e$) and glial cell depolarization is close to

Contract grant sponsor: Grant Agency of the Czech Republic; Contract grant number: 305/02/1528; Contract grant number: 305/04/1293; Contract grant sponsor: Czech Ministry of Education, Youth and Sports; Contract grant number: AV0Z5039906; Contract grant number: LN00A0650; Contract grant number: J13/98111300004.

*Correspondence to: Alexandr Chvátal, PhD, DSc, Department of Neuroscience, Institute of Experimental Medicine ASCR, Vídeňská 1083, 142 20 Praha 4, Czech Republic. E-mail: chvatal@biomed.cas.cz

Received 21 November 2002; Revised 14 June 2004; Accepted 24 June 2004

Published online 11 October 2004 in Wiley InterScience (www.interscience.wiley.com). DOI: 10.1002/jnr.20284

that predicted by the Nernst equation (Futamachi and Pedley, 1976). Further investigations, including the use of the single-channel patch-clamp technique, have shown that astrocytes and oligodendrocytes display exclusive potassium dependence of their membrane potential; therefore, these cells may be described as accurate K^+ electrodes (Walz and Hertz, 1983; Walz et al., 1984; Kettenmann et al., 1982, 1983). However, electrophysiological experiments also indicate that glial membranes might be permeable for Cl^- and that there are differences in resting Cl^- conductance between astrocytes and oligodendrocytes. A number of studies performed on cultured astrocytes revealed negligible resting Cl^- conductance (Walz and Hertz, 1983; Sonnhof, 1987; Barres et al., 1990), whereas, in cultured oligodendrocytes, a significant resting Cl^- conductance has been shown (Hoppe and Kettenmann, 1989). In addition, in experiments performed with guinea pig olfactory bulb slices, unidentified glial cells, presumably of astrocytic origin, demonstrated a passive distribution of Cl^- across their membrane and a rapid redistribution of Cl^- after a change in the driving force (Ballanyi et al., 1987). There are, however, still no convincing experimental data obtained from identified glial cells in situ on their relative permeability for K^+ and Cl^- (for review see Walz, 2002).

The first studies performed on brain slices revealed that oligodendrocytes in the corpus callosum and oligodendrocyte-like cells in the hippocampus, in contrast to oligodendrocytes in cell culture, are characterized by passive but decaying currents with prominent tail currents (I_{tail}) after the offset of a voltage jump (Berger et al., 1991; Steinhäuser et al., 1992). The application of Ba^{2+} almost completely blocked the decaying component of the inward and outward currents, as well as tail currents after depolarizing and hyperpolarizing voltage steps, indicating that these currents are carried predominantly by K^+ (Berger et al., 1991; Chvátal et al., 1995). Further analysis of oligodendrocyte currents in brain slice preparations (Chvátal et al., 1997, 1999; Vargová et al., 2001) revealed that I_{tail} observed after the offset of a depolarizing pulse are caused by the reversed shift of K^+ across the cell membrane from the ECS into the cell. Because the glial membrane is highly permeable for K^+, the membrane potential (V_m) is close to the reversal potential (V_{rev}) determined by the gradient of K^+ outside and inside the cell according to the Nernst equation. This equation has been used to determine the approximate V_{rev} immediately after membrane depolarization by using tail current analysis. In addition, the extracellular K^+ concentration ($[K^+]_e$) has been calculated from the values of V_{rev} of I_{tail} in the vicinity of the cell membrane. Based on such calculations, previous studies have indicated that membrane depolarization leads to a large K^+ increase only in the vicinity of oligodendrocytes and not around astrocytes, glial precursor cells, or neurons. In oligodendrocyte-like cells in hippocampal slices, a membrane depolarization up to +20 mV evoked a shift of V_{rev} of I_{tail} to −19 mV (Steinhäuser et al., 1992), which corresponds to 61 mM $[K^+]_e$. In a rat corpus callosum slice preparation, a depolarizing prepulse evoked an increase in $[K^+]_e$ up to 12 mM in oligodendrocyte precursors, whereas, in mature oligodendrocytes, $[K^+]_e$ reached 37 mM (Chvátal et al., 1997). In rat spinal cord slices, depolarization evoked an increase in $[K^+]_e$ up to 47 mM in oligodendrocytes, whereas, in astrocytes $[K^+]_e$ reached 12 mM, in astrocyte precursors 15 mM, and in oligodendrocyte precursors 22 mM (Chvátal et al., 1999).

In the present study, we analyzed K^+ accumulation in the vicinity of astrocytes and oligodendrocytes during and after cell depolarization, by using a modified mathematical model originally proposed for the mathematical analysis of K^+ changes in the vicinity of ventricular cells (Yasui et al., 1993). The mathematical analysis of membrane currents allowed us to calculate the volume of the extracellular space available for K^+ accumulation around glial cells and the K^+ flux from the vicinity of the glial membrane to the more distant extracellular space.

MATERIALS AND METHODS

Preparation of Rat and Mouse Spinal Cord Slices

Spinal cord slices from 22 rats and 24 mice were prepared as described previously (Chvátal et al., 1995). In brief, animals were sacrificed by decapitation under isofluran anesthesia at postnatal days 8–10 (P8–10). The spinal cords were quickly dissected out and washed in artificial cerebrospinal fluid (ACF) at 8–10°C. A 4–5-mm-long segment of the lumbar cord was embedded in 1.7% agar at 37°C (Purified Agar; Oxoid Ltd.). Transverse 200-μm-thick slices were made by using a vibroslice (OTS-4000; Electron Microscopy Sciences, Warrington, PA). Slices were individually transferred to a recording chamber mounted on the stage of a fluorescence microscope (Axioskop FX; Carl Zeiss, Jena, Germany) and fixed with a U-shaped platinum wire with a grid of nylon threads (Edwards et al., 1989). The chamber was continuously perfused with oxygenated ACF. All experiments were carried out at room temperature (~22°C).

Solutions

The ACF contained (in mM): NaCl 117.0, KCl 3.0, $CaCl_2$ 1.5, $MgCl_2$ 1.3, Na_2HPO_4 1.25, $NaHCO_3$ 35.0, D-glucose 10.0, osmolality 300 mmol/kg. The solution was continuously gassed with a mixture of 95% O_2 and 5% CO_2 to maintain a final pH of 7.4. Hypoosmotic ACF (200 mmol/kg) contained 69.0 mM NaCl. Osmolarity was measured by using a vapor pressure osmometer (Vapro 5520, Wescor Inc., Logan, UT). The perfusion rate of the ACF in the recording chamber (~2 ml volume) was 5 ml/min.

Patch-Clamp Recordings

Cell somata in the spinal cord slice were approached by the patch electrode with an Infrapatch system (Luigs & Neumann, Ratingen, Germany). The cells in the slice and the recording electrode were imaged with an infrared-sensitive video camera (C2400-03; Hamamatsu Photonics, Hamamatsu City, Japan) and displayed on a standard video monitor. Selected cells with a membrane potential more negative than −60 mV

had a clear, dark membrane surface and were located 5–10 μm below the slice surface. Membrane currents were measured with the patch-clamp technique in the whole-cell recording configuration (Hamill et al., 1981). Current signals were amplified with an EPC-9 amplifier (Heka Elektronik, Lambrecht/Pfalz, Germany), filtered at 3 kHz, and sampled at 5 kHz by an interface connected to an AT-compatible computer system, which also served as a stimulus generator.

Recording pipettes for patch-clamp recordings were pulled from borosilicate capillaries (Rückl Glass, Otvovice, Czech Republic) with a Brown-Flaming micropipette puller (P-97; Sutter Instruments Company, Novato, CA) with a tip resistance of 4–6 MΩ. The internal pipette solution had the following composition (in mM): KCl 130.0, $CaCl_2$ 0.5, $MgCl_2$ 2.0, EGTA 5.0, HEPES 10.0. The pH was adjusted with KOH to 7.2.

Immunohistochemical Identification

To visualize recorded cells in the slices, the cells were filled with either Lucifer yellow (LY) or Alexa Fluor 488 hydrazid by dialyzing the cytoplasm with the patch pipette solution. The slices were fixed with 4% paraformaldehyde in 0.1 M phosphate buffer (PB; pH 7.5) overnight at 4°C, then washed and kept in 0.1 M PB at 4°C. To distinguish between astrocytes and oligodendrocytes among the recorded cells, two markers were used: glial fibrillar acidic protein (GFAP) and S100β. Slices were incubated overnight at 4°C with a mouse monoclonal antibody directed against the subunit S100β protein (Sigma, St. Louis, MO; Donato, 1986), diluted 1:200 in PBS containing 1% bovine serum albumin (BSA) and 0.5% Triton X-100, followed by incubation with the secondary antibody, goat anti-mouse IgG conjugated with Alexa 594 (Molecular Probes, Eugene, OR) or with monoclonal antibody against GFAP conjugated with Cy3 (Sigma). After immunostaining, the slices were mounted using Vectashield mounting medium (Vector Laboratories, Burlingame, CA).

RESULTS

Experiments were performed on 59 and 82 glial cells in the gray matter of spinal cord slices of 7- and 14-day-old mice and rats, respectively. To avoid patching from motoneurons, only cells with a small soma diameter (8–15 μm) and with a membrane potential more negative than −65 mV were selected. The current patterns during de- and hyperpolarizing pulses and the morphology of cells filled with the fluorescent dyes LY or Alexa Fluor 488 hydrazid distinguished among glial cells, neurons, and glial precursor cells. Glial cells were classified on the basis of our previous electrophysiological, morphological, and immunohistochemical analyses of glial cells in rat spinal cord slices (Chvátal et al., 1995; Pastor et al., 1995). We used the following electrophysiological criteria to distinguish these cells from neurons. 1) Glial cells were identified as cells in which current pulses of up to 480 pA depolarized the cells from the holding potential of −70 mV up to +70 mV and did not activate action potentials in the current clamp mode. 2) No spontaneous electrical activity and no ability to generate action potentials were observed in glial cells.

Identification of Astrocytes and Oligodendrocytes in Spinal Cord Slices

By using the patch-clamp technique, two populations of glial cells were identified according to their membrane current patterns. The first population showed passive membrane conductance during depolarizing and hyperpolarizing voltage steps (Fig. 1), whereas the second population expressed voltage-dependent currents, namely, A-type K^+ currents, K^+ delayed rectifying and K^+ inwardly rectifying currents, and Na^+ currents (not shown). Because the mathematical model used to analyze K^+ accumulation in the vicinity of the glial membrane is affected by the presence of voltage-activated currents, these cells were excluded from the rest of the study.

For electrophysiological, morphological, and immunohistochemical identification of passive glial cells, two distinct cell types were selected: cells characterized by large, symmetrical, nondecaying selective K^+ currents during the voltage jump (Fig. 1A) and cells with symmetrical passive but decaying K^+ currents (Fig. 1B). An analysis of 58 mouse glial cells and 82 rat glial cells revealed no significant differences in glial cells expressing voltage-independent (passive) currents between the two species (Table I). Most glial cells with nondecaying currents were characterized by round cell bodies 8–10 μm in diameter and were surrounded by very fine processes that formed a diffuse network. All S100β- or GFAP-positive cells expressed such a current pattern and morphology, so these cells were identified as astrocytes. The majority of glial cells with prominent decaying currents during voltage steps had a round cell body of about 10–15 μm diameter, and, in contrast to astrocytes, these cells displayed long and parallel processes (Fig. 1B). All of these cells showing typical oligodendrocyte morphology and were negative for S100β and GFAP, a marker of astrocytes, and so were identified as oligodendrocytes (see also Gipson and Bordey, 2002). In contrast to the case for astrocytes, prominent symmetrical inward and outward tail currents (I_{tail}) could be observed after the offset of the depolarizing or hyperpolarizing voltage steps.

Further electrophysiological examination of distinct astrocytes and oligodendrocytes in both mouse and rat spinal cord slices revealed significant differences between astrocytes and oligodendrocytes (Table I). V_m was more negative in astrocytes, V_{rev} after a depolarizing prepulse was significantly shifted to positive values in oligodendrocytes, input resistance (IR) was significantly higher in oligodendrocytes, and membrane capacitance (C_m) was significantly higher in astrocytes. Because the glial cells in our experiments were characterized by high resting K^+ conductance, and the intracellular K^+ concentration ($[K^+]_i$) was controlled by the pipette solution, the Nernst equation $V = (RT/F)\ln([K^+]_e/[K^+]_i)$ was used to calculate the approximate $[K^+]$ in the vicinity of the glial membrane before (K_m) and after (K_{rev}) the depolarizing pulse and the difference as the net increase in $[K^+]$ evoked by membrane depolarization (ΔK). Our data show that a depolarizing pulse evokes a significantly larger K^+ accu-

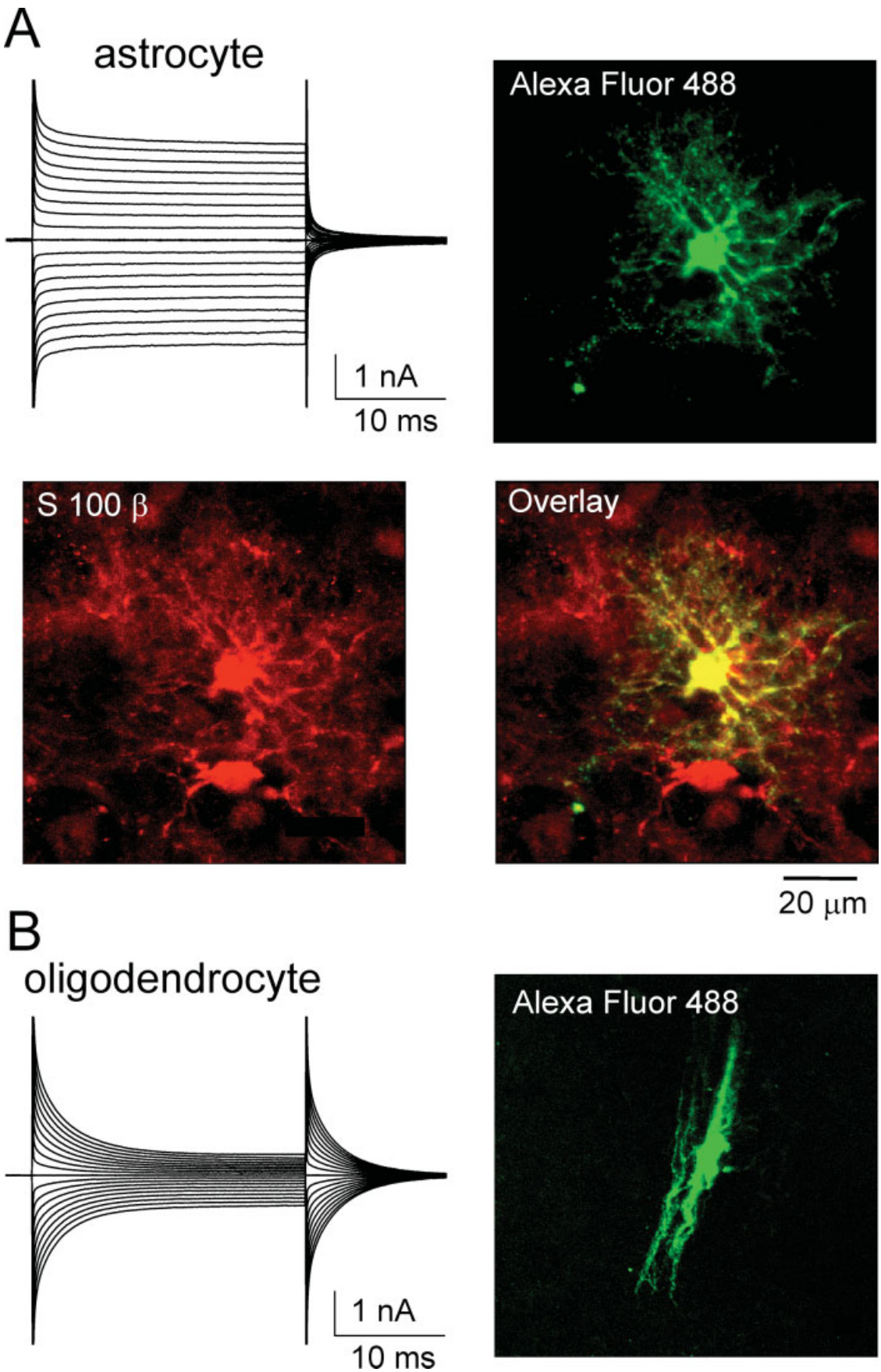
A
astrocyte
1 nA
10 ms
Alexa Fluor 488
S 100 β
Overlay
20 μm
B
oligodendrocyte
1 nA
10 ms
Alexa Fluor 488

Fig. 1.

TABLE I. Membrane Properties of Astrocytes and Oligodendrocytes in Mouse and Rat Spinal Cord Slices*

	Mice		Rats	
	Astrocytes	Oligodendrocytes	Astrocytes	Oligodendrocytes
V_m (mV)	−77.36 ± 0.64	−70.63 ± 1.40	−81.60 ± 0.88	−68.83 ± 1.45
V_{rev} (mV)	−64.00 ± 1.30	−19.95 ± 2.47	−69.36 ± 1.11	−28.94 ± 2.04
IR (mΩ)	51.59 ± 4.74	294.73 ± 25.93	59.83 ± 5.35	320.57 ± 48.10
C_m (pF)	139.09 ± 15.60	33.32 ± 4.00	173.31 ± 44.13	53.75 ± 6.11
K_m (mM)	6.15 ± 0.15	8.16 ± 0.45	5.33 ± 0.21	8.85 ± 0.55
K_{rev} (mM)	10.86 ± 0.58	63.43 ± 5.84	8.92 ± 0.42	44.40 ± 3.61
ΔK (mM)	4.71 ± 0.52	55.34 ± 5.67	3.59 ± 0.34	35.54 ± 3.54
n	39	19	59	23

*V_m, membrane potential; V_{rev}, reversal potential of the membrane after the depolarizing prepulse; IR, input resistance; C_m, membrane capacitance; K_m and K_{rev}, $[K^+]$ in the vicinity of the glial membrane calculated from the values of V_m and V_{rev}, respectively, using the Nernst equation $V = (RT/F)\ln([K^+]_e/[K^+]_i)$; ΔK, difference between K_m and K_{rev}, indicating the net increase in $[K^+]$ evoked by the depolarizing prepulse; n, number of cells. An evaluation of statistical significance revealed extremely significant differences between astrocytes and oligodendrocytes in all parameters ($P < 0.001$, unpaired, two-tailed *t*-test).

mulation in the vicinity of oligodendrocytes than in the vicinity of astrocytes (Table I). Overall, the analysis shows that glial cells with passive currents represent two distinct glial cell types with distinct membrane current patterns: astrocytes, characterized by nondecaying membrane currents during de- and hyperpolarizing voltage steps, and oligodendrocytes, characterized by a prominent current decay and by large tail currents after a voltage step.

Mathematical Model

For analyzing the K^+ accumulation evoked by a depolarizing pulse in the vicinity of glial cells, we adapted a mathematical model used to analyze K^+ accumulation in T-tubules after a depolarizing pulse in ventricular cells (Yasui et al., 1993). Our model was simplified, because, in contrast to ventricular cells or neurons, the glial membrane is characterized by high resting K^+ conductance, so only passive K^+ currents have been considered for the ion flux during membrane depolarization. The reversal potential of the glial membrane (V_{rev}) after membrane depolarization was determined from current recordings performed during a series of 20-msec test pulses ranging from −130 to +20 mV, which were preceded by a depolarizing voltage step of 90 mV, i.e., by changing the holding potential from −70 to +20 mV for 20 msec (Fig. 2A). The reversal potential of the glial membrane after the depolarizing prepulse was estimated from the current/voltage (I/V) relationship measured 5 msec after the onset of the de- and hyperpolarizing pulses (Fig. 2B). In addition to the tail current analysis, the total charge transferred across the membrane during a depolarizing pulse lasting for 40 msec (Q_{out}), and during the period of 40 msec after the offset of the depolarizing pulse (Q_{in}), was calculated from the integral of the membrane current recorded by the patch-clamp technique (Fig. 2C).

In our analysis of K^+ accumulation in the vicinity of glial cells, three compartments were considered: the intracellular space (ICS), the extracellular space in the vicinity of the cell (ESV) constrained by diffusion barriers for K^+, and the extracellular space (ECS; Fig. 2D). For simplicity, we assumed in our model that, during a depolarizing pulse, only K^+ moves out of the glial cell and accumulates in the vicinity of the membrane as a result of the high K^+ conductance. The accumulation of K^+ in the ESV is restricted by its volume (ESV_v) and by the flux of K^+ from the ESV to the areas of the ECS more distant from the cell; therefore, it was defined as:

$$J_{ve} = \frac{ESV_v}{\tau_{ve}} ([K^+]_v - [K^+]_e), \quad (1)$$

where J_{ve} is the K^+ flux between the ESV and the ECS, τ_{ve} is the time constant of the K^+ flux from the ESV to the ECS, $[K^+]_v$ is the concentration of K^+ in the ESV, and $[K^+]_e$ is the concentration of K^+ in the ECS (see Appendix for details).

$[K^+]_v$ at a given time (t) during the depolarizing pulse was calculated as follows:

Fig. 1. Membrane currents and morphology of typical astrocytes (**A**) and oligodendrocytes (**B**). Membrane currents were recorded in response to voltage steps from a holding potential of −70 mV. To activate the currents, the membrane was clamped for 50 msec to increasing de- and hyperpolarizing potentials ranging from −160 to +20 mV, at 10 mV increments. The corresponding current traces are superimposed. During recording, cells were filled with Alexa Fluor 488 by dialyzing the cytoplasm with the patch pipette solution (A, top right; B, right). After recording, the morphology of Alexa Fluor-filled cells was examined with a fluorescence microscope. In addition, the astrocyte was stained for the presence of S100β (A, bottom left); images of the Alexa Fluor-filled and S100β-stained cell are superimposed (A, bottom right).

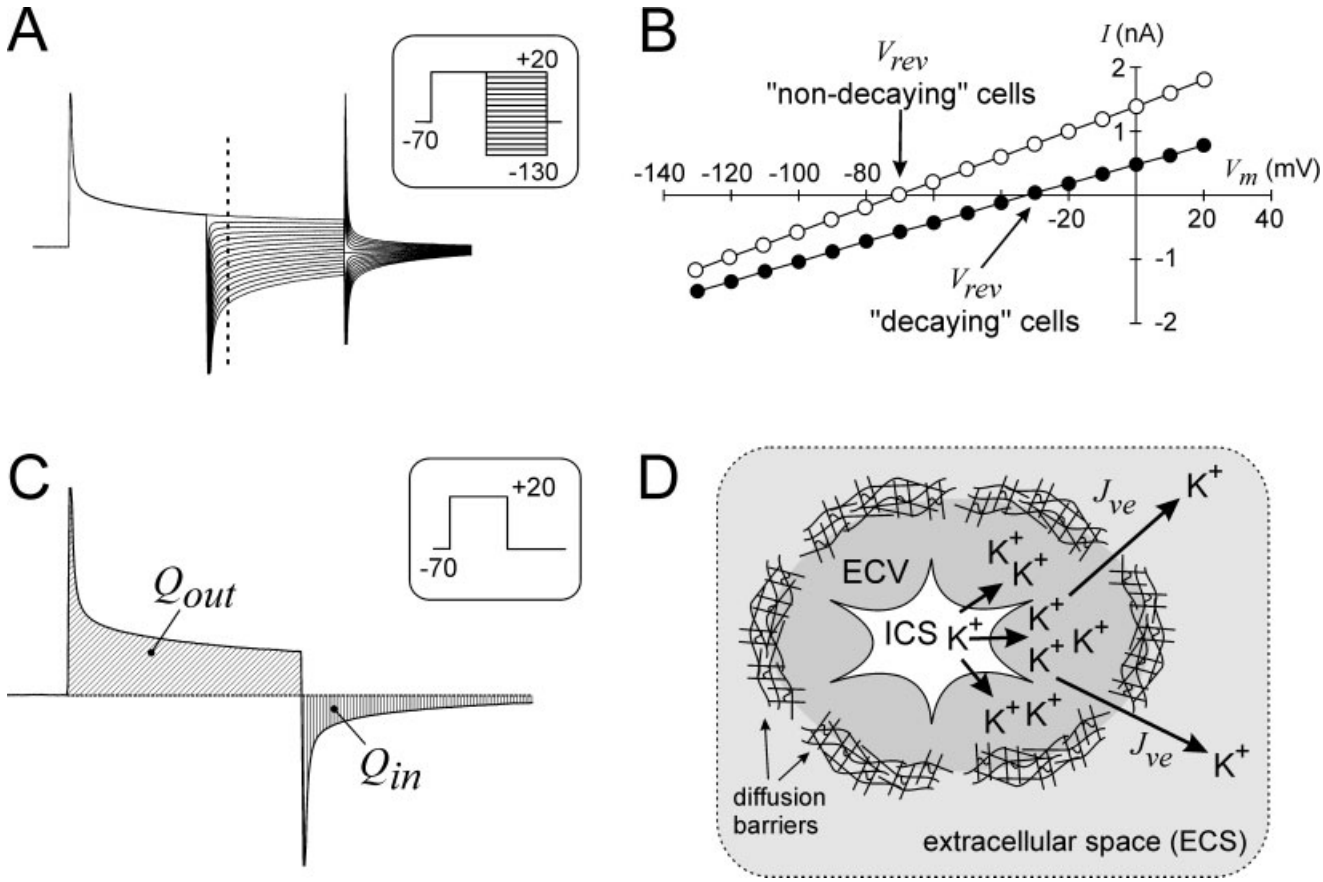

Fig. 2. Tail current analysis in astrocytes and oligodendrocytes and scheme of the mathematical model. For the tail current analysis, the membrane of an astrocyte or oligodendrocyte was clamped from a holding potential of –70 to +20 mV for 20 msec (**A**). After this prepulse, the membrane was clamped for 20 msec to increasing de- and hyperpolarizing potentials (pattern of voltage commands in **inset**) ranging from –130 to +20 mV, at 10 mV increments. From traces as shown in A, which represent recordings from a typical oligodendrocyte, currents (I) were measured five msec after the onset of the de- and hyperpolarizing pulses (dashed line) and plotted as a function of the membrane potential (V_m; **B**). The reversal potentials (V_{rev}) determined for a typical astrocyte ("non-decaying"cells) and oligodendrocyte ("decaying"cells) are indicated in the graphs by arrows. The total charge during (Q_{out}) and after a depolarizing pulse (Q_{in}) was determined as the integral of the decaying current during the 40 msec pulse from a holding potential of –70 mV to +20 mV (pattern of voltage commands in **inset**) and during 40 msec after the offset of the depolarizing pulse (**C**). Scheme of the mathematical model used to calculate the volume of the ECS available for K^+ accumulation in the vicinity of the glial membrane (**D**). ICS, intracellular space; ESV, space in the vicinity of the cell; J_{ve}, ionic flux between the ESV and ECS. For further explanation, see text.

$$[K^+]_v = [K^+]_{v,\infty} - ([K^+]_{v,\infty} - [K^+]_{v,0})\exp\left(-\frac{t}{\tau_{ve}}\right), \quad (2)$$

where $[K^+]_{v,\infty}$ is the steady-state $[K^+]$ in the ESV at time $t = \infty$, and $[K^+]_{v,0}$ is the $[K^+]$ in the ESV during the holding potential at time $t = 0$, i.e., before the depolarizing pulse.

$[K^+]_{v,\infty}$ was defined as:

$$[K^+]_{v,\infty} = \frac{I\tau_{ve}}{F \cdot ESV_v} + [K^+]_e, \quad (3)$$

where I is the current recorded at the glial membrane during the depolarizing pulse and F is Faraday's constant.

The calculation of $[K^+]$ in the ESV at the end of the depolarizing pulse was based on the Nernst equation, where the membrane potential of the cell was equal to the reversal potential (V_{rev}) defined as:

$$V_{rev} = \frac{RT}{F} \ln\left(\frac{[K^+]_{v,rev}}{[K^+]_i}\right), \quad (4)$$

where R is the gas constant, T is temperature, $[K^+]_{v,rev}$ is the $[K^+]$ in the ESV at the end of the depolarizing pulse, and $[K^+]_i$ is the intracellular $[K^+]$. V_{rev} of glial cells after a depolarizing pulse was calculated by using tail current analysis (Berger et al., 1991; Chvátal et al., 1999; Fig. 2A,B); $[K^+]_i$ was determined by the composition of the solution in the patch pipette, and $[K^+]_{v,rev}$ was calculated using Equation 4 as:

$$[K^+]_{v,rev} = [K^+]_i \exp\left(\frac{V_{rev}F}{RT}\right). \quad (5)$$

Our previous studies indicated that the current decrease during a voltage step in oligodendrocytes is produced by K^+ accumulation in the vicinity of the cell membrane; therefore, before fitting procedures, a section of the current trace between the second and twentieth milliseconds of depolarization was converted to the equivalent of $[K^+]_e$ (Fig. 3A,B). The membrane current during a depolarizing pulse can be defined using Ohm's law as:

$$I = \frac{U}{W}, \quad (6)$$

where U is the membrane potential and W is the resistance of the glial membrane. The membrane current at any given time can therefore be defined using the modified Equations 4 and 6 as follows:

$$I = \frac{\frac{RT}{F}\ln\left(\frac{[K^+]_i}{[K^+]_v}\right)}{W}. \quad (7)$$

Equation 7 indicates the relationship between the K^+ gradient across the glial membrane and the membrane current during a depolarizing pulse. With increasing values of $[K^+]_v$, membrane current decreases (Fig. 3, top inset). When, theoretically, $[K^+]_v = [K^+]_i$, then $I = 0$. The membrane current I measured by the patch electrode was converted to values of $[K^+]_{v,c}$ by using Equation 7 as follows:

$$[K^+]_{v,c} = \frac{[K^+]_i}{\exp\left(\frac{IWF}{\xi RT}\right)}, \quad (8)$$

where $[K^+]_{v,c}$ is the $[K^+]_v$ converted from the values of I, and the value of parameter ξ was adjusted to equalize $[K^+]_{v,c}$ at the end of the depolarizing pulse, with $[K^+]_{v,rev}$ calculated from the values of V_{rev} after the depolarizing pulse (Fig. 3C).

A fitting procedure was used to find the best solution to the combination of Equations 2 and 3 by varying the values of τ_{ve}, ESV_v, and $[K^+]_{v,0}$ (Fig. 3D–G). At the beginning, the initial values of ESV_v, τ_{ve}, and $[K^+]_{v,0}$ were introduced into these equations. The value of $[K^+]$ at the end of the depolarizing pulse was found by varying the τ_{ve} (Fig. 3D). The time course of K^+ accumulation in the ESV, indicated in Figure 3E by the shape of the curves, is determined by the volume of the ESV; therefore, as the second step, the value of ESV_v was found that best matched the original curve. For every new value of ESV_v, it was necessary to recalculate a new, corresponding value of τ_{ve}. Surprisingly, under normal conditions, the values of $[K^+]_{v,0}$

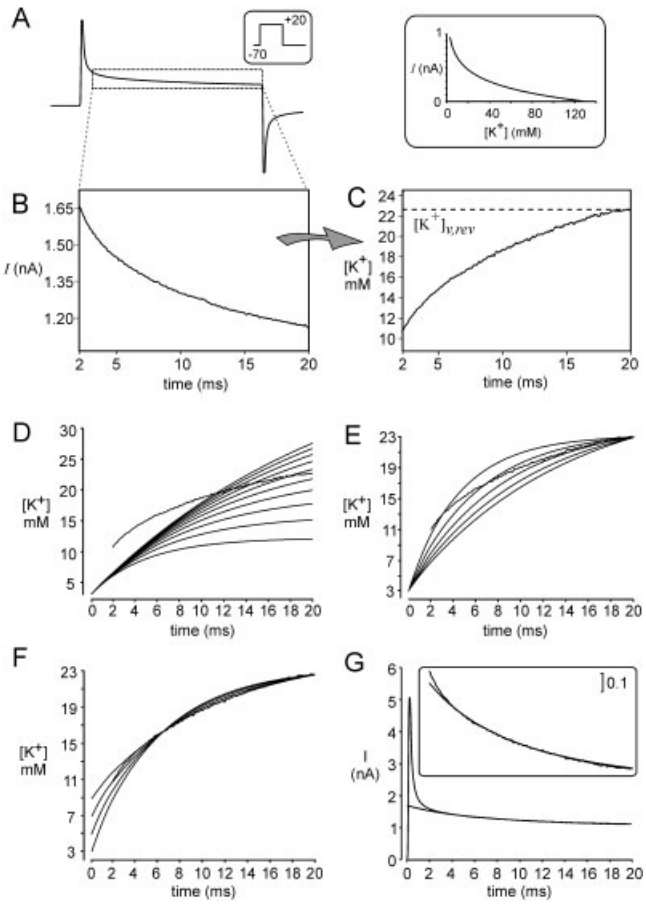

Fig. 3. Conversion of membrane current to $[K^+]_e$ in the vicinity of the glial membrane (**A–C**) and fitting procedure (**D–G**). A portion of the membrane current between 2 and 20 msec (dotted lines) recorded during cell depolarization from a holding potential of −70 to +20 mV for 20 msec (A,B) was converted to the corresponding values of $[K^+]_e$ using Equation 8 (C). The dashed line in C indicates the extracellular concentration of K^+ calculated from the membrane reversal potential after the depolarizing pulse using the Nernst equation. **Inset:** Relation between membrane current and extracellular K^+ concentration according to Equation 7. Fitting procedure (D): The concentration of K^+ in the vicinity of the cell at the end of the depolarizing pulse is defined by τ_{ve}. The initial values of $ESV_v = 70^{-18}$ m^3 and $[K^+]_{v,0} = 3$ mM were introduced into Equations 2 and 3, and the corresponding value of τ_{ve} was determined by increasing the value of τ_{ve} in 2-msec steps. The speed of K^+ accumulation (the shape of the fitting curve) is determined by the ESV_v; therefore, the value of ESV_v was calculated after matching the best fit to the original curve (E). For every new value of ESV_v, it was necessary to recalculate the corresponding value of τ_{ve}. The value of ESV_v was decreased in 10^{-18} m^3 steps. The best fit was found when the value of $[K^+]_{v,0}$, i.e., the initial value of $[K^+]$ in the vicinity of the membrane at the beginning of the depolarizing pulse, was adjusted to higher values than the concentration in the ACF, 3 mM (F). For every new value of $[K^+]_{v,0}$, the corresponding values of τ_{ve} and ESV_v were recalculated. The value of $[K^+]_{v,0}$ was increased in 2 mM steps. The significance of the fit was checked after converting the values of $[K^+]$ to the current equivalents using Equation 7 and superpositioning them on the original current traces (G). Increased magnification of the original current recording and the theoretical curve are shown in the **inset**.

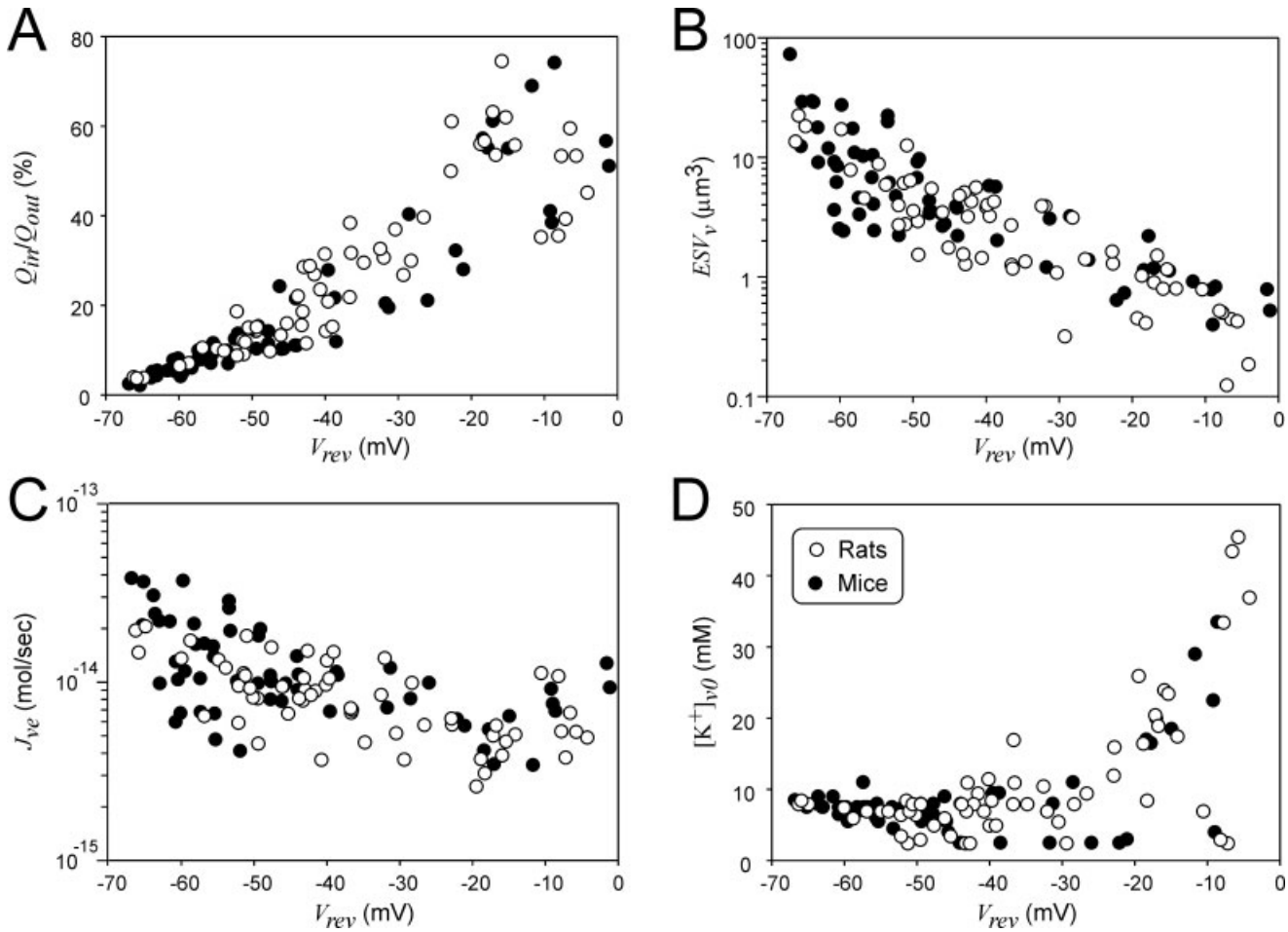

Fig. 4. Experimental data obtained from membrane currents recorded in astrocytes and oligodendrocytes in rat and mouse spinal cord slices. The relation between the reversal potential (V_{rev}) after a depolarizing pulse and the Q_{in}/Q_{out} ratio, expressed as a percentage (**A**); the ESV volume (ESV_v; **B**); the K^+ flux from the ESV to the ECS (J_{ve}; **C**); and the initial value of $[K^+]$ in the vicinity of the membrane at the beginning of the depolarizing pulse ($[K^+]_{v,0}$; **D**). Note that, with increasing values of V_{rev}, the Q_{in}/Q_{out} ratio increased and the values of ESV_v and J_{ve} decreased. Higher values of $[K^+]_{v,0}$ were obtained only in cells with more positive V_{rev}.

usually did not match the values of the resting $[K^+]_e$ (3–4 mM) found experimentally in the spinal cord by using ion-selective microelectrodes (for review see Syková, 1992); instead, in most cases, the best fit was found when the value of $[K^+]_{v,0}$ was adjusted to higher values (Fig. 3F). For every new value of $[K^+]_{v,0}$, the corresponding values of τ_{ve} and ESV_v had to be recalculated. The significance of the fit was determined after conversion of the $[K^+]$ values to the equivalent of current I using Equation 7 and after superimposition onto the original current traces (Fig. 3G). From the values of τ_{ve}, ESV_v, and $[K^+]_v$, the value of the K^+ flux between the ESV and the ECS (J_{ve}) was calculated using Equation 1.

K^+ Accumulation in the Vicinity of Glial Cells

For the mathematical analysis of K^+ accumulation in the vicinity of the glial membrane, all glial cell types with passive currents, including cells with a current pattern intermediate between astrocytes and oligodendrocytes, were analyzed in the gray matter of 7–14-day-old rat (n = 59) and mouse (n = 60) spinal cord slices. The following parameters were determined: reversal potential after a depolarizing pulse (V_{rev}), the volume of the ESV (ESV_v), the K^+ flux between the ESV and the ECS (J_{ve}), and the $[K^+]$ in the ESV before the depolarizing prepulse ($[K^+]_{v,0}$). In addition, the values of V_{rev} were also correlated with the total charge during the inward current after the depolarizing pulse (Fig. 4).

There were no significant differences in the results obtained from rats vs. mice. More positive values of V_{rev} evoked by membrane depolarization are accompanied by a greater charge transferred across the membrane during the inward current (Q_{in}) after the offset of the depolarizing pulse (Fig. 4A). The charge during the inward current was normalized for all cells as a percentage of the total charge evoked by the outward current (Q_{out}) during the depo-

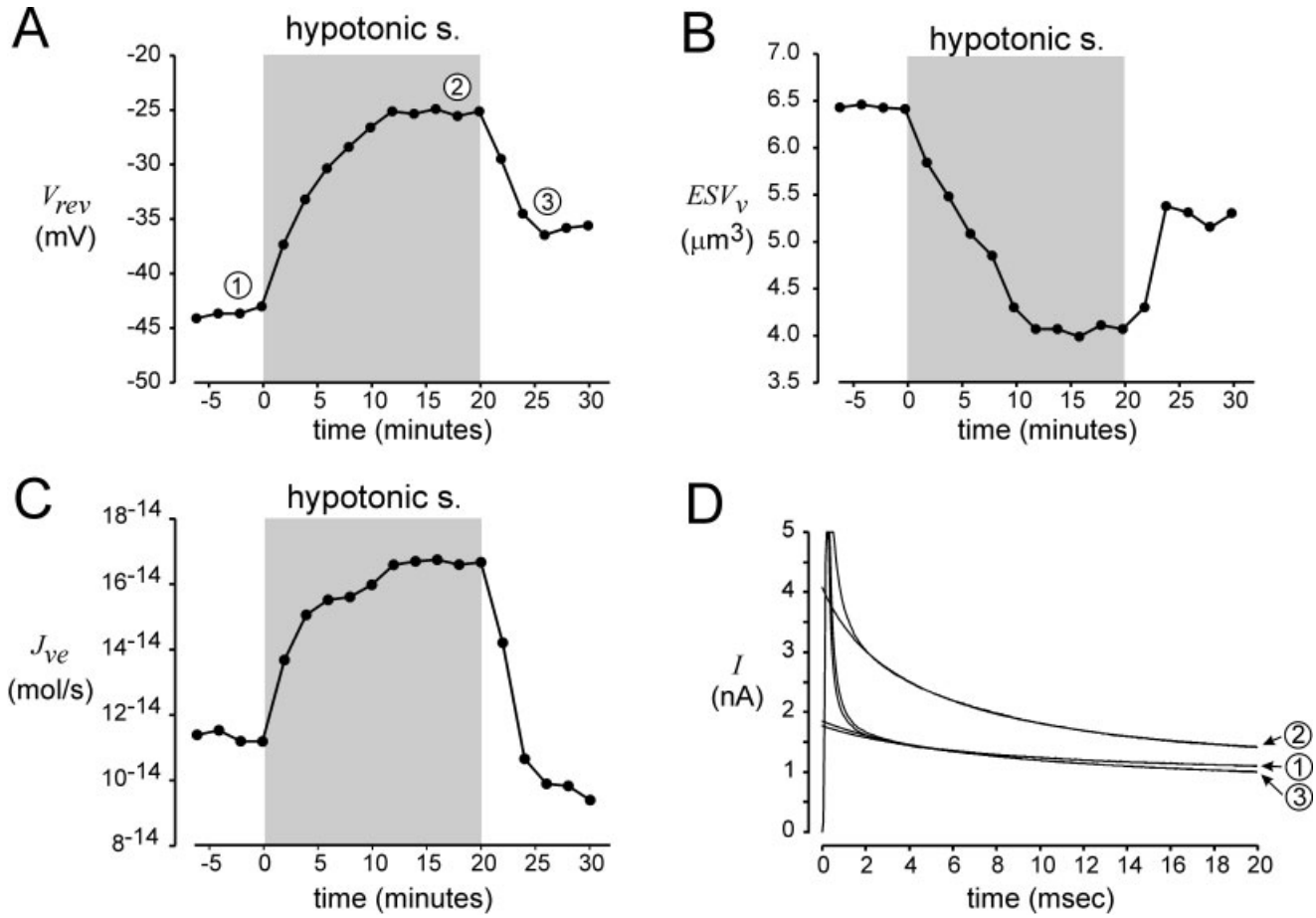

Fig. 5. An example of the changes in a cell exposed to hypotonic stress. Hypotonic solution (200 mmol/kg) evoked a shift in the reversal potential (V_{rev}) from −44 to −27 mV (**A**). An increase in V_{rev} is accompanied by a decrease in ESV volume (ESV_v; **B**) and by an increase in the K^+ flux from the ESV to the ECS (J_{ve}; **C**). An example of superimposed experimental and theoretical curves obtained before (1), during (2) and after (3) exposure to hypotonic solution is shown in **D**.

larizing pulse and was expressed as $(Q_{in}/Q_{out}) \times 100\%$. In cells with V_{rev} from −70 to −50 mV, Q_{in}/Q_{out} was not greater than 20%, whereas, in cells with V_{rev} from −20 to 0 mV, it was 30–70%.

The analysis of membrane currents with our mathematical model showed that more positive values of the reversal potential are accompanied by a smaller ESV volume in the vicinity of the glial membrane (Fig. 4B). For cells with a reversal potential ranging from −70 to −50 mV, presumably astrocytes, the typical values of ESV_v were in the range of 2–50 μm^3, whereas, for cells with a V_{rev} ranging from −20 to 0 mV, presumably oligodendrocytes, the values of ESV_v were 0.1–2 μm^3.

Our analysis also shows that the K^+ flux from the ESV to the ECS is dependent on the V_{rev} (Fig. 4C). With increasing values of V_{rev} from −70 to 0 mV, the values of J_{ve} decreased from 2×10^{-13} to 3×10^{-14} mol/sec, respectively. K^+ flux between the ESV and ECS is therefore lower around those glial cells surrounded by a more compact extracellular space available for K^+ accumulation.

The mathematical analysis of current recordings revealed that, in cells with a reversal potential more negative than −30 mV, the resting level of $[K^+]$ in the vicinity of the glial membrane ($[K^+]_{v,0}$) did not exceed 10 mM $[K^+]_e$ (Fig. 4D). However, in a number of cells with a V_{rev} more positive than −30 mV, $[K^+]_{v,0}$ was significantly greater and rose up to 47 mM.

To study the changes in K^+ flux and accumulation in the vicinity of the glial membrane during cell swelling, spinal cord slices were exposed to hypotonic stress (see also Vargová et al., 2001). In astrocyte-like cells during the application of 200 mmol/kg for 20 min, the reversal potential evoked by a depolarization pulse rose by 17.2 ± 1.8 mV (n = 5; Fig. 5). The values of ESV_v and J_{ve} were calculated from the membrane current recordings before (Fig. 5, 1), during (Fig. 5, 2), and after

(Fig. 5, 3) the exposure of the cell to hypotonic solution. A shift of the reversal potential to positive values was accompanied not only by the accumulation of K^+, as calculated from the Nernst equation, but also by a decrease in ESV_v of $3.6 \pm 1.3\ \mu m^3$ and by an increase in the K^+ flux from the ESV to the ECS of $4-8 \times 10^{-14}$ mol · s^{-1}.

DISCUSSION

Passive Glial Cells Are Astrocytes and Oligodendrocytes With High Resting K^+ Conductance

Our mathematical analysis shows differences in K^+ accumulation in the vicinity of the membranes of glial cells expressing passive currents in the gray matter of mouse and rat spinal cord slices. In the present study, the identification of these cells was in accordance with our previous studies (Chvátal et al., 1995), and the cells were identified immunohistochemically and electrophysiologically as astrocytes or oligodendrocytes. However, some studies indicate that, as a result of cell treatment during measurements, at least passive astrocytes might not represent a distinct population, insofar as a spillage of pipette solution containing low Ca^{2+}/EGTA during cell approach in slice recordings and/or poor cell access can lead to a transient masking of voltage-activated currents, even in cells that express prominent voltage-activated currents (Bordey and Sontheimer, 1998). On the other hand, many studies performed in different regions of the brain in situ have revealed the presence of passive as well as complex glial cells (Steinhäuser et al., 1994; Chvátal et al., 1995; Jabs et al., 1997; D'Ambrosio et al., 1998; Zawar et al., 1999). Therefore, it seems most likely that passive and complex cells represent two extremes of one highly plastic astrocyte type (for review see Walz, 2000).

Pioneering studies of the electrophysiological properties of glial cells in leech ganglia (Kuffler et al., 1966; Orkand et al., 1966) and the subsequent analysis of cultured astrocytes (Bevan et al., 1985; Sonnhof, 1987; Barres et al., 1990; Jalonen, 1993; Lascola and Kraig, 1996) revealed a high resting K^+ conductance and no evidence for significant Cl^- activity at resting potentials (for review see Walz, 2002). There are, however, some indications that, in some populations of oligodendrocytes in culture (Hoppe and Kettenman, 1989) and in a population of unidentified glial cells, presumably astrocytes, in guinea pig olfactory bulb slices (Ballanyi et al., 1987), a change in membrane potential may elicit an equilibration of Cl^- evoked by changes in the driving force. Convincing data on the relative membrane permeability for K^+ and Cl^- in glial cells in situ is still lacking and will require further experiments on identified glial cells in brain slices. It was generally accepted that astrocytes have a negligible resting Cl^- conductance, whereas oligodendrocytes may display a small accumulation of Cl^- with a relatively larger resting Cl^- conductance than seen in astrocytes; the Cl^- conductance in astrocytes can, however, be up-regulated during changes in activity states, such as injury or neoplasia (Walz, 2002). In addition, previous experiments performed in mouse brain and rat spinal cord in situ revealed that the decaying current component during a de- or hyperpolarizing pulse, as well as tail currents after the pulse, are in oligodendrocytes almost completely blocked by the application of Ba^{2+} (Berger et al., 1991; Chvátal et al., 1995). We can therefore conclude that the major membrane current component in our experiments is mediated by K^+ and that the changes in tail currents reflect an accumulation of K^+ in the vicinity of the glial membrane, although a relatively small contribution of other conductances cannot be excluded.

Mechanisms of K^+ Shift Across the Glial Membrane Evoked by Changes in Membrane Potential

The proposed model of K^+ accumulation in the vicinity of astrocytes and oligodendrocytes used in the current study supports the hypothesis that oligodendrocytes are surrounded by a smaller extracellular space available for K^+ accumulation than are astrocytes (Berger et al., 1991; Steinhäuser et al., 1992; Chvátal et al., 1997, 1999, 2001; Anděrová et al., 2001; Vargová et al., 2001). Depolarization of the oligodendrocyte membrane produces a significant shift in membrane reversal potential to positive values, and, because the glial membrane is highly permeable to K^+, this shift is caused by the large accumulation of potassium in the vicinity of the oligodendrocyte membrane. An increasing $[K^+]_e$ is accompanied by a decrease in the $[K^+]_e/[K^+]_i$ gradient, so a current decrease is observed during membrane depolarization. Tail currents after the offset of the depolarizing pulse are produced by the reversed flux of K^+ back into the cell. Such a feature of oligodendrocytes has been observed in different areas of the CNS in different animal species, but not in cultured cells (Sontheimer and Kettenmann, 1988; Sontheimer et al., 1989), so it is evident that K^+ accumulation and its concomitant movement into cells are determined by the properties of the nervous tissue, especially by the properties of the extracellular space, not present in cell cultures. Our analysis of the fraction of the ECS where K^+ accumulates during a depolarizing pulse, the flux of K^+ from the vicinity of the cell to the ECS, and the resting level of K^+ near the cell membrane revealed the presence of a large ECS available for K^+ accumulation in the vicinity of astrocytes but a 10–100 times smaller ECS available for K^+ accumulation in the vicinity of oligodendrocytes. In addition, K^+ flux from the space close to the cell membrane to the more distant areas of the ECS is facilitated around astrocytes.

Is Accumulation of K^+ in the Vicinity of the Glial Membrane Related to the Size of the ECS?

The question remains of how the accumulation of K^+ is related to changes in glial cell volume and the size of intercellular clefts. The morphology of nerve cells is very complex and includes shaped cell bodies and processes surrounded by a variable ECS. However, several simplifications allow us to obtain rough estimates of the spatial

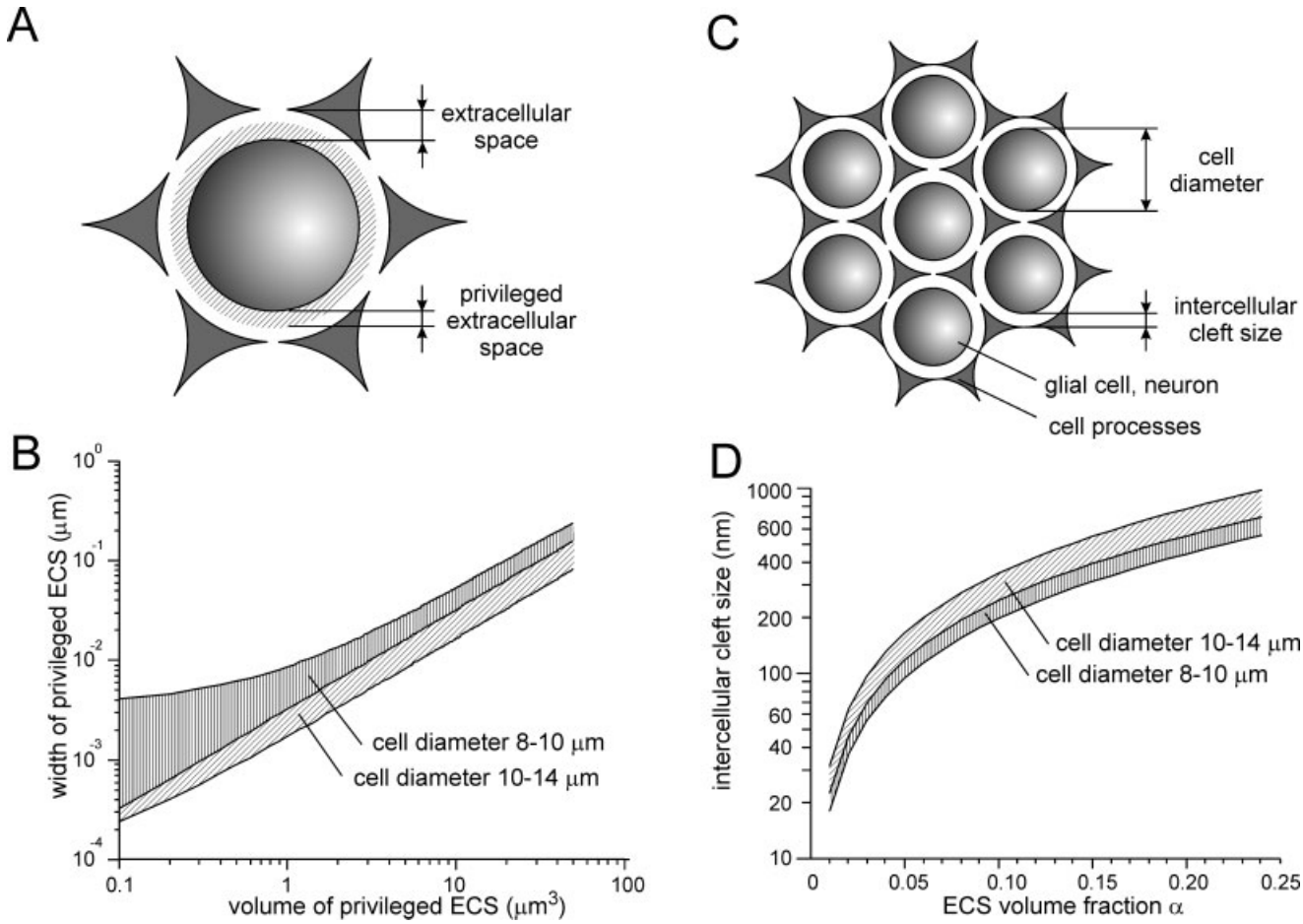

Fig. 6. Theoretical calculations of the width of the privileged extracellular space in the vicinity of glial cells (**A,B**) and the cleft size of the extracellular space (ECS; **C,D**). Data were calculated for the average cell diameter of astrocytes (8–10 μm) and oligodendrocytes (10–14 μm), determined experimentally. Triangular structures in A represent cell membranes surrounding the particular cell with the adjacent intracellular space, whereas in C these structures represent cell processes. For further explanation, see text.

characteristics of the space in the vicinity of the glial membrane. First, we can consider only glial cell bodies, insofar as, because of insufficient space-clamp of cells and the higher electrical resistance of astrocyte and oligodendrocyte processes, the membrane current recorded by the patch-clamp technique may arise mainly from the cell bodies. There are no experimental data for the space-clamp conditions in spinal cord glial cells; however, studies performed on hippocampal slices indicate that, as a result of poor space-clamp associated with recording from cells with a highly intricate morphology, voltage steps applied to the glial cell soma do not influence the membrane potential of fine distal processes (D'Ambrosio et al., 1999). The diameters of astrocyte and oligodendrocyte cell bodies in the spinal cord gray matter are 8–10 μm and 10–14 μm, respectively (Chvátal et al., 1995; Vargová et al., 2001). Assuming for simplicity a circular cell body with an average diameter of 10 μm, cell volume is 524 μm^3. The calculated volumes of the ECS available for K^+ accumulation in the vicinity of glial cells, therefore, ranged from 0.2 μm^3 in oligodendrocytes to 50 μm^3 in astrocytes; i.e., the width of such a space around oligodendrocytes is 0.3–10 nm and that around astrocytes 4–154 nm (Fig. 6A,B).

One of the first attempts to link tail currents with K^+ accumulation and intercellular cleft size was made in a study by Frankenhaeuser and Hodgkin (1956) of the aftereffects of impulses in the giant nerve fibers of *Loligo*. Calculations made from the potassium increase indicated that it should accumulate in a space 27 nm wide between an axon and a Schwann cell. Similar values were also used later in the Adelman-Palti (1972) model of ion accumulation in the periaxonal space. The role of glial cells in potassium accumulation in the extracellular space was examined by using a mathematical model by Lebovitz (1970), who also considered the intermembrane separa-

tions between neurons and glial cells to range between 5 and 50 nm, because electron microscopy studies indicated that the separation between adjacent membranes in the CNS is less than 50 nm (Lebovitz, 1970). These models used to describe K^+ accumulation were based on electron microscopy and fixation techniques that did not preserve the ECS, so the intercellular cleft size in these studies was artificially small. However, reevaluated calculations using new data and a modified mathematical model (Astion et al., 1988) showed that, in contrast to the original results obtained by Frankenhaeuser and Hodgkin, i.e., a cleft size of 25–30 nm, the same intercellular clefts are much wider and can even approach 200 nm. These clefts are not uniform and may vary over a range of 0.2–200 nm.

For the CNS, recent data from electron microscopy techniques that preserve the ECS (Tian et al., 1991), radiotracer methods (Levin et al., 1970), and particularly in vivo measurements with the real-time iontophoretic method (Nicholson and Philips, 1981) indicate that the average ECS volume is about 20–24% of the brain volume; i.e., the ECS volume fraction, defined as the ratio of the ECS volume to the total volume of the brain, is 0.20–0.24 (for reviews see Nicholson and Syková, 1998; Nicholson, 2001). During pathological situations, such as ischemia or anoxia, however, the ECS volume fraction can decrease dramatically to 0.03–0.05 (for reviews see Syková et al., 2000; Syková, 2001). For a rough estimate of the relationship between the intercellular clefts in a tissue with a large number of cell bodies, i.e., gray matter, and different values of the ECS volume, a modified equation introduced originally by Reichenbach (1991) for the outer nuclear layer of the retina can by used:

$$w = \frac{1}{2}\left(\frac{d}{\sqrt[3]{1 - \frac{\alpha\sqrt{18}}{\pi}}} - d\right), \qquad (9)$$

where w is the intercellular cleft width, d is the diameter of the cell, and α is the ECS volume fraction. In comparison with nervous tissue, the model is simplified; i.e., the intercellular clefts and cell bodies are circular, they have the same size, and the space between cells is filled with cell processes (Fig. 6C). However, the model shows that, in tissue with an extracellular volume fraction of 0.24, the intercellular cleft size between cells with a diameter of 8–14 μm is 500–1,000 nm, i.e., much larger than the size estimated from the electron microscopy studies in which the ECS is not preserved (Fig. 6D).

Validity of the Proposed Mathematical Model

Our results indicate that there is a discrepancy between the size of the ECS available for K^+ accumulation around the two types of glial cells and the size of the intercellular clefts calculated using Reichebach's model for cells with a diameter in the range of 8–14 μm. The size of the ECS available for K^+ accumulation in the vicinity of round cells with a diameter of 10 μm is only 0.4% of the size of intercellular cleft around oligodendrocytes, whereas, around astrocytes, it is 4.3%. There are several explanations for these differences: 1) There could be inaccurate calculations resulting from simplifications of the mathematical model; 2) the ECS volume fraction determined by the real-time iontophoretic method represents an average of the ECS volume in nervous tissue over a region of 10^{-3} mm^3, and it could differ in the vicinity of individual cells; and 3) the privileged ECS for K^+ accumulation in the vicinity of the cell membrane occupies only a fraction of the ECS. In addition, inaccurate calculations may also arise from an overestimation of the cell body diameter of glial cells, because the estimates are based on images of cells filled with the fluorescent dye LY or Alexa Fluor 488 hydrazid. Strong fluorescence of the soma in comparison with the processes could lead to overexposure and to overestimation of somatic diameters (see also Chvátal et al., 1995). Use of smaller cell body diameters in the calculations results in a greater size of the privileged region of the ECS (see Fig. 6A). Another possibility could be different cleft sizes around oligodendrocytes and astrocytes where the boundaries of the ECS are formed by the membranes of adjacent cells. Heterogeneities in the ECS volume have been found in different areas of the brain and spinal cord with the real-time iontophoretic method (Syková, 1997; Nicholson and Syková, 1998). Heterogeneities could also be present in the vicinity of different glial cell types. As was described by Penfield (1924), nonmyelinating oligodendrocytes in the gray matter, in contrast to astrocytes, are usually located in the convexity of the neuronal cell body, and a narrow intercellular cleft can be observed between oligodendrocytes and neurons. In addition, oligodendrocyte processes often pass over the surface of a neuron. K^+ flux in the ECS can be restricted by diffusion barriers that are part of the extracellular space, i.e., by charged particles, adhesion molecules, and molecules of the extracellular matrix (ECM). Since ECM molecules in the brain form perineuronal nets and are synthesized by glial cells (Brückner et al., 1993, 1996; Viggiano et al., 2000), their presence close to the cell membrane can affect the diffusion and/or accumulation of K^+ in the vicinity of glial cells. It was shown that perineuronal proteoglycans may form a perineuronal gel layer that protects the synapses as a "perisynaptic barrier" (Murakami and Ohtsuka, 2003). ECM molecules can therefore also be involved in boundary formation between the privileged ECS region in the vicinity of glial cells and other regions of the ECS.

We conclude that an analysis of K^+ shifts following the depolarization of the glial membrane reveals a privileged region of the ECS in the vicinity of glial cells available for K^+ accumulation. This region of the ECS is more than 10 times smaller around oligodendrocytes than around astrocytes and such a difference may be due to either morphological differences between astrocytes and oligodendrocytes or to the presence of diffusion barriers formed by the constituents of the ECS, e.g., charged molecules, adhesion molecules, or molecules of the ECM.

The concept of a privileged ECS around cells is not new, Virchow (1858) having suggested the presence of cell territories (Zellenterritorien) in the "intercellular substance which is dependent in a certain definite manner upon the cells . . . and it is necessary to draw boundaries in it also, so that certain districts belong to one cell, and certain others to another." The presence of such diffusion barriers in the CNS may also affect, in addition to K^+, the accumulation and diffusion of other neuroactive substances and alter extrasynaptic communication between cells.

ACKNOWLEDGMENT

The authors thank Tomáš Mazel for his participation in the preparation of the Appendix.

REFERENCES

Adelman WJ Jr, Palti Y. 1972. The role of periaxonal and perineuronal spaces in modyfying ionic flows across neural membranes. In: Bronner F, Kleinzeller A, editors. Current topics in membrane transport. New York: Academic Press. p 199–235.

Agnati LF, Zoli M, Strömberg I, Fuxe K. 1995. Intercellular communication in the brain: wiring versus volume transmission. Neuroscience 69: 711–726.

Anděrová M, Kubinová Š, Mazel T, Chvátal A, Eliasson C, Pekny M, Syková E. 2001. Effect of elevated K^+, hypotonic stress and cortical spreading depression on astrocyte swelling in GFAP-deficient mouse. Glia 35:189–203.

Astion ML, Coles JA, Orkand RK, Abbott NJ. 1988. K^+ accumulation in the space between giant axon and Schwann cell in the squid *Alloteuthis*. Effects of changes in osmolarity. Biophys J 53:281–285.

Ballanyi K, Grafe P, Ten Bruggencate G. 1987. Ion activities and potassium uptake mechanisms of glial cells in guinea-pig olfactory cortex slices. J Physiol 382:159–174.

Barres BA, Koroshetz WJ, Chun LLY, Corey DP. 1990. Ion channel expression by white matter glia: the type-1 astrocyte. Neuron 5:527–544.

Berger T, Schnitzer J, Kettenmann H. 1991. Developmental changes in the membrane current pattern, K^+ buffer capacity and morphology of glial cells in the corpus callosum slice. J Neurosci 11:3008–3024.

Bevan S, Chiu SY, Gray PTA, Ritchie JM. 1985. The presence of voltage-gated sodium, potassium and chloride channels in rat cultured astrocytes. Proc R Soc Lond B Biol Sci 225:299–313.

Bordey A, Sontheimer H. 1998. Passive glial cells, fact or artifact? J Membrane Biol 166:213–222.

Brückner G, Brauer K, Hartig W, Wolff JR, Rickmann MJ, Derouiche A, Delpech B, Girard N, Oertel WH, Reichenbach A. 1993. Perineuronal nets provide a polyanionic, glia-associated form of microenvironment around certain neurons in many parts of the rat brain. Glia 8:183–200.

Brückner G, Hartig W, Kacza J, Seeger J, Welt K, Brauer K. 1996. Extracellular matrix organization in various regions of the rat brain grey matter. J Neurocytol 25:333–346.

Chvátal A, Syková E. 2000. Glial influence on neuronal signaling. Prog Brain Res 125:199–216.

Chvátal A, Pastor A, Mauch M, Syková E, Kettenmann H. 1995. Distinct populations of identified glial cells in the developing rat spinal cord: Ion channel properties and cell morphology. Eur J Neurosci 7:129–142.

Chvátal A, Berger T, Vořišek I, Orkand RK, Kettenmann H, Syková E. 1997. Changes in glial K^+ currents with decreased extracellular volume in developing rat white matter. J Neurosci Res 49:98–106.

Chvátal A, Anděrová M, Žiak D, Syková E. 1999. Glial depolarization evokes a larger potassium accumulation around oligodendrocytes than around astrocytes in gray matter of rat spinal cord slices. J Neurosci Res 56:493–505.

Chvátal A, Anděrová M, Žiak D, Orkand RK, Syková E. 2001. Membrane currents and morphological properties of neurons and glial cells in the spinal cord and filum terminale of the frog. Neurosci Res 40:23–35.

D'Ambrosio R, Wenzel J, Schwartzkroin PA, McKhann GM, Janigro D. 1998. Functional specialization and topographic segregation of hippocampal astrocytes. J Neurosci 18:4425–4438.

D'Ambrosio R, Maris DO, Grady MS, Winn HR, Janigro D. 1999. Impaired K^+ homeostasis and altered electrophysiological properties of post-traumatic hippocampal glia. J Neurosci 19:8152–8162.

Donato R. 1986. S-100 proteins. Cell Calcium 7:123–145.

Edwards FA, Konnerth A, Sakmann B, Takahashi T. 1989. A thin slice preparation for patch clamp recordings from neurones of the mammalian central nervous system. Pflügers Arch 414:600–612.

Frankenhaeuser B, Hodgkin AL. 1956. The after-effects of impulses in the giant nerve fibres of *Loligo*. J Physiol 131:341–376.

Futamachi KJ, Pedley TA. 1976. Glial cells and extracellular potassium: their relationship in mammalian cortex. Brain Res 109:311–322.

Gipson K, Bordey A. 2002. Analysis of the K^+ current profile of mature rat oligodendrocytes in situ. J Membrane Biol 189:201–212.

Hamill OP, Marty A, Neher E, Sakmann B, Sigworth FJ. 1981. Improved patch-clamp techniques for high-resolution current recording from cells and cell-free membrane patches. Pflügers Arch 391:85–100.

Hoppe D, Kettenmann H. 1989. Carrier-mediated chloride transport in cultured mouse oligodendrocytes. J Neurosci Res 23:467–475.

Jabs R, Paterson IA, Walz W. 1997. Qualitative analysis of membrane currents in glial cells from normal and gliotic tissue in situ. Neuroscience 81:847–860.

Jalonen T. 1993. Single-channel characteristics of the large-conductance anion channel in rat cortical astrocytes in primary culture. Glia 9:227–237.

Kettenmann H, Orkand RK, Lux HD, Schachner M. 1982. Single potassium channel currents in cultured mouse oligodendrocytes. Neurosci Lett 32:41–46.

Kettenmann H, Sonnhof U, Schachner M. 1983. Exclusive potassium dependence of the membrane potential in cultured mouse oligodendrocytes. J Neurosci 3:500–505.

Kuffler SW, Nicholls JG, Orkand RK. 1966. Physiological properties of glial cells in the central nervous system of amphibia. J Neurophysiol 29:768–787.

Lascola CD, Kraig RP. 1996. Whole-cell chloride currents in rat astrocytes accompany changes in cell morphology. J Neurosci 16:2532–2545.

Lebovitz RM. 1970. A theoretical examination of ionic interactions between neural and non-neural membranes. Biophys J 10:423–444.

Levin VA, Fenstermacher JD, Patlak CS. 1970. Sucrose and inulin space measurements of cerebral cortex in four mammalian species. Am J Physiol 219:1528–1533.

Murakami T, Ohtsuka A. 2003. Perisynaptic barrier of proteoglycans in the mature brain and spinal cord. Arch Histol Cytol 66:195–207.

Nicholson C. 2001. Diffusion and related transport mechanisms in brain tissue. Rep Prog Phys 64:815–884.

Nicholson C, Phillips JM. 1981. Ion diffusion modified by tortuosity and volume fraction in the extracellular microenvironment of the rat cerebellum. J Physiol 321:225–257.

Nicholson C, Syková E. 1998. Extracellular space structure revealed by diffusion analysis. Trends Neurosci 21:207–215.

Orkand RK, Nicholls JG, Kuffler SW. 1966. Effect of nerve impulses on the membrane potential of glial cells in the central nervous system of amphibia. J Neurophysiol 29:788–806.

Pastor A, Chvátal A, Syková E, Kettenmann H. 1995. Glycine- and GABA-activated currents in identified glial cells of the developing rat spinal cord slice. Eur J Neurosci 7:1188–1198.

Penfield W. 1924. Oligodendroglia and its relation to classical neuroglia. Brain 47:430–452.

Reichenbach A. 1991. Glial K^+ permeability and CNS K^+ clearance by diffusion and spatial buffering. Ann N Y Acad Sci 633:272–286.

Sonnhof U. 1987. Single voltage-dependent potassium and chloride channels in cultured astrocytes. Can J Physiol Pharmacol 65:1043–1050.
Sontheimer H, Kettenmann H. 1988. Heterogeneity of potassium currents in cultured oligodendrocytes. Glia 1:415–420.
Sontheimer H, Trotter J, Schachner M, Kettenmann H. 1989. Channel expression correlates with differentiation stage during the development of oligodendrocytes from their precursor cells in culture. Neuron 2:1135–1145.
Steinhäuser C, Berger T, Frotscher M, Kettenmann H. 1992. Heterogeneity in the membrane current pattern of identified glial cells in the hippocampal slice. Eur J Neurosci 4:472–484.
Steinhäuser C, Jabs R, Kettemann H. 1994. Properties of GABA and glutamate responses in identified glial cells of the mouse hippocampal slice. Hippocampus 4:19–35.
Syková E. 1992. Ionic and volume changes in the microenvironment of nerve and receptor cells. In: Ottoson D, editor. Progress in sensory physiology, vol 13. Heidelberg: Springer. p 1–176.
Syková E. 1997. The extracellular space in the CNS: its regulation, volume and geometry in normal and pathological neuronal function. Neuroscientist 3:28–41.
Syková E. 2001. Glial diffusion barriers during aging and pathological states. Prog Brain Res 132:339–363.
Syková E, Mazel T, Vargová L, Vořišek I, Prokopová Š. 2000. Extracellular space diffusion and pathological states. Prog Brain Res 125:155–178.
Tian M, Reger JF, Armstrong WE. 1991. Electron microscopic and immunocytochemical study of rapidly frozen, freeze-substituted neural lobes of rats. J Neurocytol 20:79–96.
Vargová L, Chvátal A, Anděrová M, Kubinová Š, Žiak D, Syková E. 2001. Effect of osmotic stress on potassium accumulation around glial cells and extracellular space volume in rat spinal cord slices. J Neurosci Res 65:129–138.
Viggiano D, Ibrahim M, Celio MR. 2000. Relationship between glia and the perineuronal nets of extracellular matrix in the rat cerebral cortex: importance for volume transmission in the brain. Prog Brain Res 125: 193–198.
Virchow R. 1858. Cellularpathologie in ihre Begründung auf Physiologische un Pathologishe Gewebelehre. Berlin: A. Hirschwald [translated Chance F (1863) Philadelphia: J.B. Lipincott & Co.; reprinted (1971) New York: Dover].
Walz W. 2000. Controversy surrounding the existence of dicrete functional classes of astrocytes in adult gray matter. Glia 31:95–103.
Walz W. 2002. Chloride/anion channels in glial cell membranes. Glia 40:1–10.
Walz W, Hertz L. 1983. Comparison between fluxes of potassium and of chloride in astrocytes in primary cultures. Brain Res 277:321–328.
Walz W, Wuttke W, Hertz L. 1984. Astrocytes in primary cultures: membrane potential characteristics reveal exclusive potassium conductance and potaccium accumulation properties. Brain Res 292:367–374.
Yasui K, Anno T, Kamiya K, Boyett MR, Kodama I, Toyama J. 1993. Contribution of potassium accumulation in narrow extracellular spaces to the genesis of nicorandil-induced large inward tail current in guinea-pig ventricular cells. Pflügers Arch 422:371–379.
Zawar C, Plant TD, Schirra C, Konnerth A, Neumcke B. 1999. Cell-type specific expression of ATP-sensitive potassium channels in the rat hippocampus. J Physiol 514:327–341.
Zoli M, Jansson A, Syková E, Agnati LF, Fuxe K. 1999. Volume transmission in the CNS and its relevance for neuropsychopharmacology. Trends Pharmacol Sci 20:142–150.

APPENDIX

K^+ accumulation in the vicinity of the glial membrane is affected by the flux of K^+ across diffusion barriers between the ESV and the ECS. As indicated in Figure 3A, the permeability of diffusion barriers for K^+ is different around astrocytes and oligodendrocytes. Less permeable barriers around oligodendrocytes, in contrast to astrocytes, produce greater K^+ accumulation, so the total charge carried by K^+ into the cell during tail currents is also greater. Changes in $[K^+]$ in the volume of the ESV ($[K]_v$) can, therefore, be defined as:

$$ESV_v \frac{d[K^+]_v}{dt} = J_{iv} - J_{ve}, \quad (A1)$$

where ESV_v is the volume of the ESV, $d[K^+]/dt$ is the change of $[K^+]$ during time dt, J_{iv} is the K^+ flux across the cell membrane from the cell into the ESV, and J_{ve} is the K^+ flux between the ESV and the ECS (Fig. 7A). J_{iv} is defined as:

$$J_{iv} = \frac{I}{F}, \quad (A2)$$

where I is the membrane K^+ current and F is the Faraday's constant. J_{ve} may be expressed in terms of Fick's diffusion equation. According to Fick's law:

$$j = -D \frac{[K^+]_e - [K^+]_v}{w}, \quad (A3)$$

where D is the diffusion coefficient of K^+ diffusing through a boundary with a width, w. Because j is the K^+ flux from the ESV volume per unit time and unit surface, the total K^+ flux through surface S per unit volume is defined as:

$$J_{ve} = j \cdot S = \frac{D \cdot S}{w} ([K^+]_v - [K^+]_e). \quad (A4)$$

Equation A1 may now be expressed as:

$$\frac{d[K^+]_v}{dt} + \frac{D \cdot S}{w \cdot ESV_v} ([K^+]_v - [K^+]_e) = \frac{I}{F \cdot ESV_v} \quad (A5)$$

or

$$\frac{d[K]_v}{dt} + \frac{D \cdot S}{w \cdot ESV_v} \left([K]_v - [K]_e - \frac{I \cdot w \cdot ESV_v}{F \cdot ESV_v \cdot D \cdot s} \right) = 0. \quad (A6)$$

The solution to Equation A6 can be found through the following steps:

1. separation of variables:

$$\frac{d[K]_v}{\left([K]_v - [K]_e - \frac{I \cdot w \cdot ESV_v}{F \cdot V \cdot D \cdot S} \right)} = -\frac{D \cdot S}{w \cdot ESV_v} \cdot dt, \quad (A7)$$

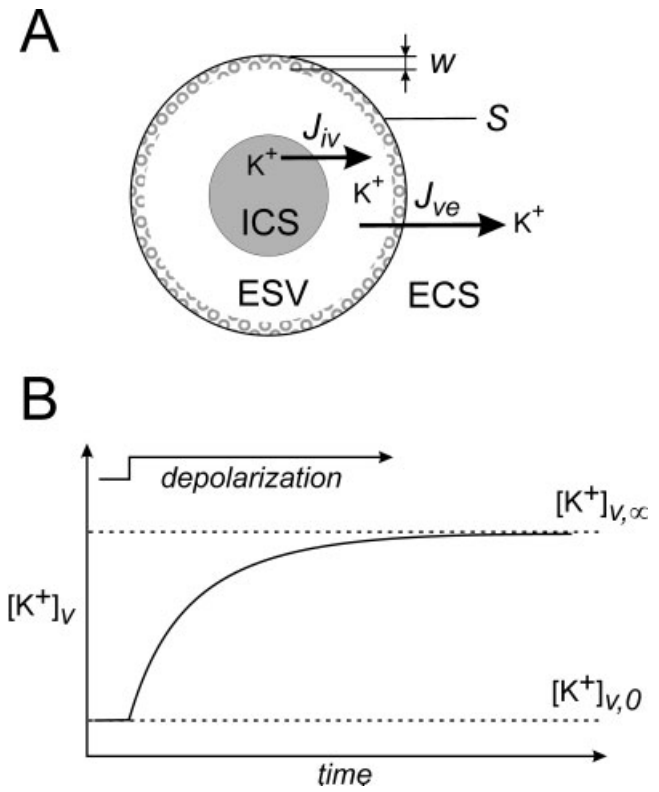

Fig. 7. Theoretical considerations for the mathematical modeling of the K^+ flux from a glial cell during depolarization (**A**) and the theoretical time course of changes in $[K^+]$ in the vicinity of a cell (**B**). ICS, intracelluar space; ESV, space in the vicinity of the cell membrane; ECS, extracellular space; J_{iv}, ion flux from ICS to ESV; J_{ve}, ion flux from ESV to ECS; S, boundary surface; w, boundary width. For further explanation, see Appendix.

2. integration:

$$\ln\left([K]_v - [K]_e - \frac{I \cdot w \cdot ESV_v}{F \cdot ESV_v \cdot D \cdot S}\right) = \frac{t}{\tau_{ve}} + \ln c, \quad (A8)$$

where $\tau_{ve} = w \cdot ESV_v/D \cdot S$ and c is the integration constant.

3. taking the exponential:

$$\left([K]_v - [K]_e - \frac{I \cdot w \cdot ESV_v}{F \cdot ESV_v \cdot D \cdot S}\right) = c \cdot \exp\left(-\frac{t}{\tau_{ve}}\right), \quad (A9)$$

and, therefore,

$$[K]_v = c \cdot \exp\left(-\frac{t}{\tau_{ve}}\right) + [K]_e + \frac{I \cdot w \cdot ESV_v}{F \cdot ESV_v \cdot D \cdot S}. \quad (A10)$$

For $t = \infty$, i.e., during steady state, when $J_{iv} = J_{ve}$, no changes in $[K^+]_v$ occur (Fig. 7B), and, therefore,

$$[K]_{v,\infty} = \frac{I \cdot \tau_{ve}}{F \cdot ESV_v} + [K]_e \quad (A11)$$

at time $t = 0$:

$$[K]_{v,0} = c + \frac{I \cdot \tau_{ve}}{F \cdot ESV_v} + [K]_e = [K]_e, \quad (A12)$$

and, therefore,

$$c = -\frac{I \cdot \tau_{ve}}{F \cdot ESV_v} = [K]_{v,0} - [K]_{v,\infty}. \quad (A13)$$

Thus the solution of Equation A5 can be written as:

$$[K]_v = [K]_{v,\infty} - ([K]_{v,\infty} - [K]_{v,0})\exp\left(-\frac{t}{\tau_{ve}}\right). \quad (A14)$$